Kato et al. Nanoscale Research Letters (2017) 12:242
DOI 10.1186/s11671-017-2006-z

Nanoscale Research Letters

NANO EXPRESS Open Access

Influence of Fabrication Processes and Annealing Treatment on the Minority Carrier Lifetime of Silicon Nanowire Films

Shinya Kato[1*], Tatsuya Yamazaki[2], Yasuyoshi Kurokawa[3], Shinsuke Miyajima[4] and Makoto Konagai[5,6]

Abstract

Surface passivation and bulk carrier lifetime of silicon nanowires (SiNWs) are essential for their application in solar cell devices. The effective minority carrier lifetime of a semiconductor material is influenced by both its surface passivation and bulk carrier lifetime. We found that the effective carrier lifetime of SiNWs passivated with aluminum oxide (Al_2O_3) was significantly influenced by the fabrication process of SiNWs. We could not measure the effective lifetime of SiNWs fabricated by thermal annealing of amorphous silicon nanowires. Nevertheless, the SiNWs fabricated by metal-assisted chemical etching of polycrystalline silicon displayed an effective lifetime of 2.86 μs. Thermal annealing of SiNWs at 400 °C in a forming gas improved the effective carrier lifetime from 2.86 to 15.9 μs because of the improvement in surface passivation at the interface between the SiNWs and Al_2O_3 layers.

Keywords: Silicon nanowire, Passivation, Minority carrier lifetime

Background

Silicon nanowires (SiNWs) possess promising qualities for use in thin-film solar cells, i.e., they exhibit a strong optical confinement effect that is essential for light trapping in solar cells [1–5]. SiNWs can be fabricated by metal-assisted chemical etching (MAE), which is a low-cost chemical solution-based process and, therefore, presents a potential for low-cost fabrication of SiNW-based solar cells [6–11]. Carrier recombination can significantly affect the performance of solar cells. Thus, the application of SiNWs in solar cells will require the carrier recombination in SiNWs to be examined. One of the most important measures of carrier recombination is the effective carrier lifetime (τ_{eff}). The value of τ_{eff} is very sensitive to the surface recombination and bulk lifetime, and therefore, τ_{eff} measurements provide information about surface recombination and bulk lifetime at the same time [12–14]. Owing to the difficulties with the fabrication of isolated SiNWs, however, only few studies examining the τ_{eff} of SiNWs have been reported in the literature to date [15, 16]. SiNWs are often fabricated by chemical etching of a crystalline Si (c-Si) substrate [6, 17]. In SiNWs fabricated using the proposed method, the c-Si substrate remains underneath the SiNWs and influences the outcome of τ_{eff} measurements. For this reason, fabrication techniques that do not employ the c-Si wafer are needed to remove the influence of the c-Si substrate on the τ_{eff} measurements of SiNWs.

In our previous work, isolated SiNWs were fabricated from polycrystalline Si (poly-Si) on a quartz substrate [7–9]. Additionally, our previous work also demonstrated that τ_{eff} measurements of isolated SiNWs and their optical characterization are possible [15].

In this study, we investigated the influence of the fabrication process of isolated SiNWs passivated with aluminum oxide (Al_2O_3) on τ_{eff}. Isolated SiNWs can be fabricated using two different processes, as shown in Fig. 1. Here, SiNWs were fabricated by thermal annealing of amorphous silicon (a-Si) nanowires, marked in Fig. 1 as process A. The a-Si nanowires were fabricated using the MAE process. Additionally, SiNWs were fabricated by MAE of poly-Si, in a process marked as B in Fig. 1. In this case, the poly-Si layer was fabricated by thermal annealing of an a-Si layer. Finally, the influence of annealing time and temperature on the value of τ_{eff} was investigated.

* Correspondence: kato.shinya@nitech.ac.jp
[1]Department of Electrical and Mechanical Engineering, Nagoya Institute of Technology, Showa-ku, Nagoya-shi, Aichi 466-8555, Japan
Full list of author information is available at the end of the article

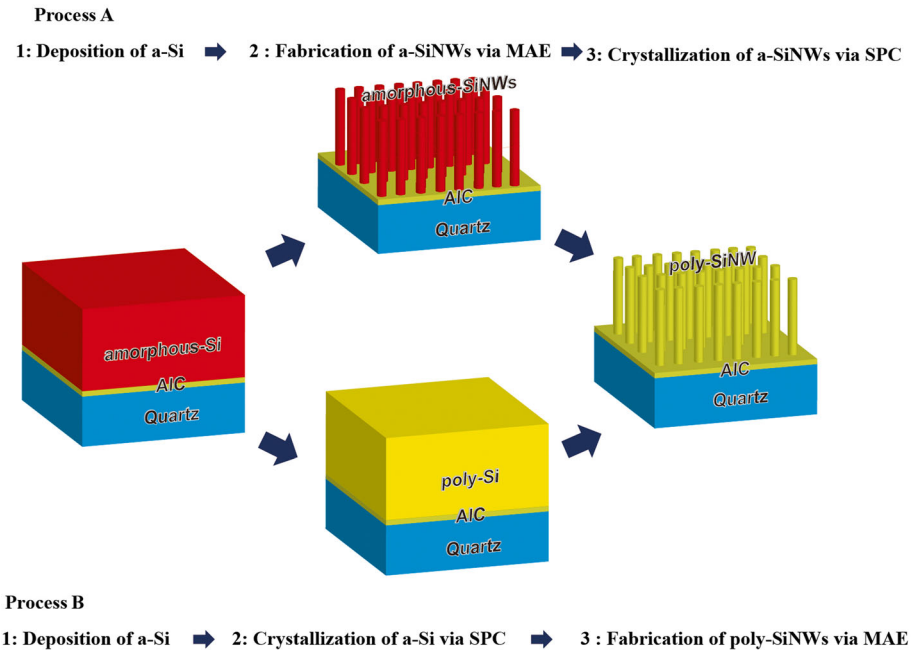

Fig. 1 Two different fabrication processes of a poly-SiNW

Methods

Isolated SiNWs were fabricated using two different procedures as shown in Fig. 1. A highly doped thin poly-Si layer of thickness 163 nm was fabricated on a quartz substrate by aluminum-induced crystallization (AIC). The details of the AIC process have been reported previously [8]. The AIC-poly-Si layer acts as a seed layer for the crystallization of SiNWs. Subsequently, an intrinsic a-Si (i-a-Si) layer was deposited on the AIC-poly-Si by radio frequency sputtering. In process A, amorphous SiNWs were fabricated by MAE of the i-a-Si layer. During the MAE process, silver particles were deposited on the i-a-Si layer by electroless silver plating. The sample containing silver nanoparticles was immersed in an etching solution comprising HF and H_2O_2. Following the formation of amorphous SiNWs, the sample was dipped in an HNO_3 solution to remove the silver nanoparticles. Finally, the oxide layer formed on the surface of the amorphous SiNWs was removed using an HF solution. The amorphous SiNWs were crystallized by thermal annealing at 800, 900, and 1000 °C for 30 min in a forming gas (FG) under ambient conditions. In process B, the i-a-Si layer was crystallized by solid phase crystallization (SPC) to give the poly-Si prior to nanowire formation through thermal annealing at 900 °C for 30 min in a forming gas at ambient conditions. Finally, the SiNWs were fabricated from the poly-Si layer by MAE.

Following the preparation of SiNWs, an Al_2O_3 layer was deposited on the SiNWs for surface passivation by atomic layer deposition. As reported in [6], the effective lifetime of SiNWs lacking a passivation layer cannot be measured because of the extremely high effective surface recombination velocity. Figure 2 depicts the cross-sectional image obtained by using a scanning electron microscope (SEM) and the energy dispersive X-ray spectroscopy (EDS) images of SiNWs containing an Al_2O_3 layer. The EDS images clearly showed that the signals arising from Al and O are observed uniformly across the entire area of the sample. This result indicates that the fabricated SiNWs were entirely covered with the Al_2O_3 layer. Thermal annealing treatment was conducted in a forming gas (4% H_2 in N_2) at 300, 400, and 500 °C. The influence of annealing time on the passivation quality was also investigated.

The structure of the fabricated SiNW samples was characterized by field-emission SEM (FE-SEM) and EDS (JEOL, JSM-7001F). The crystallization of SiNWs was confirmed by Raman spectroscopy (JASCO, NRS-1000, excitation wavelength of 532 nm). The effective carrier lifetime of the samples was measured using a microwave photoconductivity decay (MWPCD) technique and a 904-nm laser (KOBELCO, LTE-1510EP). The interface-state density (D_{it}) and fixed-charge density (Q_{ss}) were measured using a noncontact corona-voltage (C-V) technique (SEMILAB Co. Ltd., PV-2000).

Results and Discussion

Figure 3 depicts the cross-sectional SEM images of SiNWs fabricated using process A and process B. The shape of the wires was found to be very similar for both

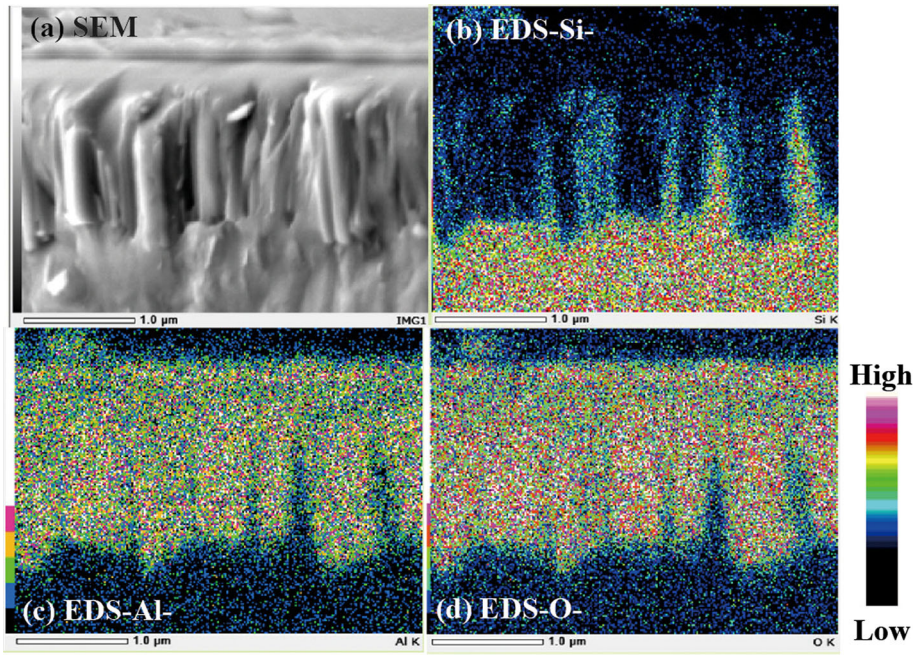

Fig. 2 Cross-sectional SEM and EDS images of a-SiNW sample after deposition of Al_2O_3. **a** SEM image. **b** EDS image for Si. **c** EDS image for Al. **d** EDS image for O

processes, indicating that similar patterns of silver nanoparticles were formed on both the i-a-Si and poly-Si layers. This result demonstrated that the Ag pattern does not depend on the employed fabrication process. In the next step, the internal structure of SiNWs fabricated using different procedures was investigated by Raman spectroscopy. Figure 4a depicts the Raman spectra of SiNWs fabricated using process A. The Raman spectra of SiNWs crystallized at 800, 900, and 1000 °C are shown in Fig. 4a. Three peaks, attributed to crystalline silicon (peak 1), nanocrystalline silicon (peak 2), and amorphous silicon (peak 3), were observed in all spectra. In contrast, only peaks 1 and 2 were observed in the spectra of SiNWs fabricated using process B (Fig. 4b). These results indicate that the SiNWs fabricated using process A contained a residual a-Si phase. The results of Raman spectroscopy, therefore, suggest that the crystallization temperature of a-SiNWs is higher than that of a-Si. This temperature difference can be explained by the Helmholtz free energy of poly-Si. When a polycrystalline silicon with a radius r is prepared, the change in the Helmholtz free energy can be calculated as shown in Eq. (1).

$$\Delta F = -\frac{4}{3}\pi r^3 \Delta F_v + 4\pi\sigma r^2 \tag{1}$$

where ΔF_v is the variation in Helmholtz free energy between a-Si and poly-Si per unit volume and σ is the interface energy. The first term represents the variation in free energy because of phase transformation from a-Si to poly-Si, and therefore, ΔF is expected to become negative as the poly-Si grows. The second term represents the increase in the surface area of a-Si that results in the free energy increase. When the influence of the

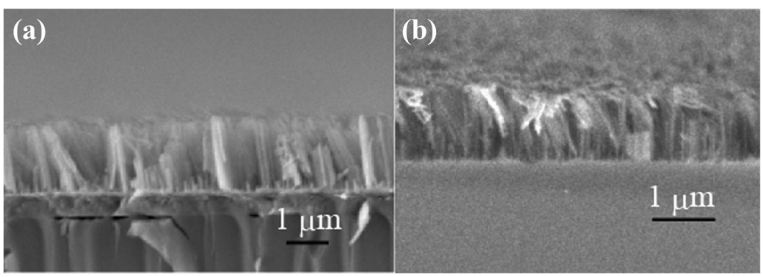

Fig. 3 Cross-sectional SEM image of the SiNWs. **a** Process A. **b** Process B

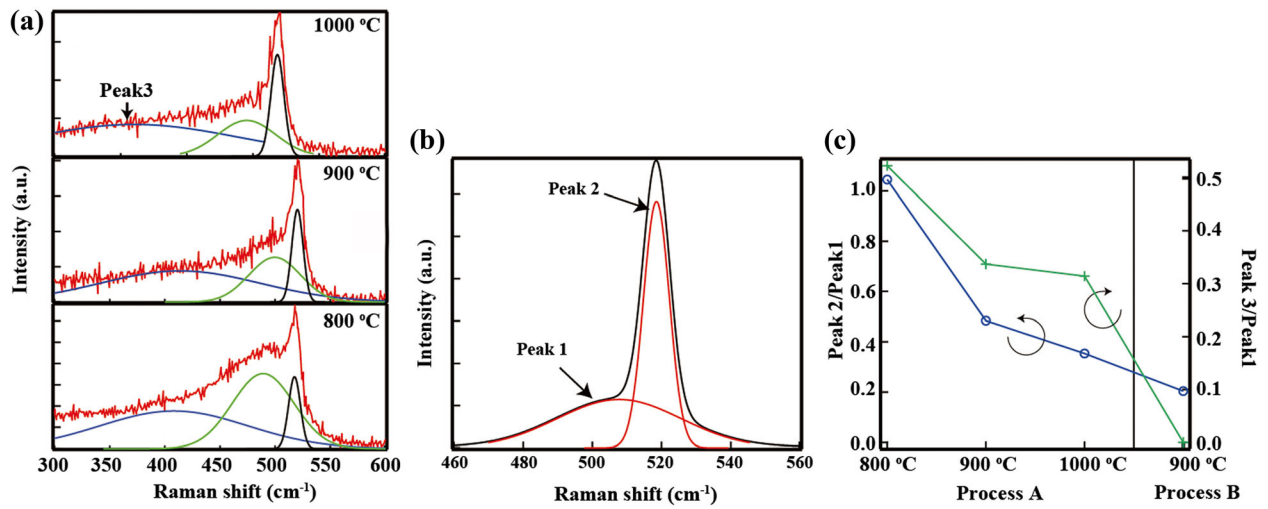

Fig. 4 **a** Raman spectra of SiNW fabricated by process A at 800, 900, and 1000 °C. **b** Raman spectra of SiNW fabricated by process B at 900 °C. **c** The ratio of Peak 2/Peak 1 and Peak 3/Peak 1

second term is stronger than that of the first term, the a-Si does not crystallize. The crystal nucleation in a-SiNW is affected easily by the nanowire surface, and therefore, the second term is larger than the first term. As a result, the crystallization temperature of a-SiNW is higher compared with that of a-Si. To date, a number of studies reported in the literature have shown that the crystallization temperature of a-Si nanostructure increases [18–20].

In addition to structural characterization, we investigated the τ_{eff} of SiNWs/Al_2O_3 fabricated using different procedures. The results showed that the τ_{eff} of SiNWs/Al_2O_3 fabricated using process A could not be measured, whereas that of SiNWs/Al_2O_3 fabricated using process B was successfully measured. Most likely, this difference can be attributed to the bulk lifetime of SiNWs since the surface passivation quality of SiNWs fabricated using both processes was essentially identical. The results of Raman spectroscopy confirmed the presence of a residual a-Si phase in the SiNWs fabricated using process A, and this presence significantly affects the bulk lifetime of SiNWs. Overall, these results indicate that process B is more useful for solar cell applications than process A.

The surface passivation quality of the c-Si/Al_2O_3 interface is known to be strongly influenced by thermal annealing. Therefore, we investigated the effect of thermal annealing on the τ_{eff} of SiNWs/Al_2O_3 fabricated using process B. Figure 5 depicts the decay curves of the MWPCD signal of as-deposited and annealed SiNWs/Al_2O_3. Each decay curve can be divided into fast and slow decay components. Although the origin of the slow decay has not been clarified, it is most likely related to the carrier trap in SiNWs. We estimated the τ_{eff} of as-deposited SiNWs/Al_2O_3 from the fast decay curve as 2.86 μs. Thermal annealing of SiNWs/Al_2O_3 at 400 °C

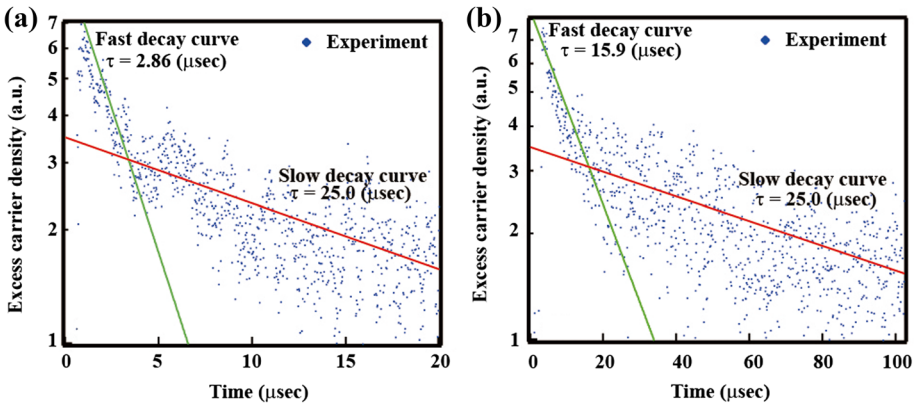

Fig. 5 Decay curve of MWPCD signal of SiNW/Al_2O_3 sample **a** before and **b** after thermal annealing

for 30 min in the forming gas increased the τ_{eff} drastically from 2.86 to 15.9 μs.

Generally, the surface recombination velocity of the Si and Al_2O_3 interface decreases during thermal annealing because of the formation of a negative fixed charge [21–24]. Therefore, we examined the effect of thermal annealing on the SiNW/Al_2O_3 samples in more detail. Figure 6a depicts the variation in τ_{eff} observed as a function of annealing time and temperature. For annealing temperatures of 300 and 400 °C, the τ_{eff} increased as the annealing time was increased to 30 min, followed by a region of saturation. Interestingly, the behavior exhibited by τ_{eff} at the annealing temperature of 500 °C was very different from that exhibited by τ_{eff} at other temperatures. The annealing at 500 °C for 1 min increased the τ_{eff} from 3 to 11 μs. However, further increase in annealing time resulted in a monotonic decrease in τ_{eff}. The difference in behavior observed at the low annealing temperatures (300 and 400 °C) and the high temperature (500 °C) can be attributed to the changes in surface passivation. Figure 6b depicts the changes in τ_{eff} of c-Si/Al_2O_3 determined as a function of annealing time and temperature. This experiment was performed to examine the influence of annealing on the quality of surface passivation. To eliminate the influence of bulk lifetime, we employed a monocrystalline Si substrate (p-type, [100], 8–12 Ωcm, thickness of 550 μm). The results showed that annealing at 400 °C increased the τ_{eff} monotonically, whereas annealing at 500 °C decreased the τ_{eff} after a long annealing time. Overall, the behavior observed for the τ_{eff} of c-Si/Al_2O_3 was similar to that determined for SiNWs/Al_2O_3. The τ_{eff} of c-Si/Al_2O_3 samples is known to be determined by D_{it} and Q_{ss}. Nevertheless, determining D_{it} and Q_{ss} at the interface of SiNWs/Al_2O_3 is extremely challenging, and therefore, we estimated these parameters from those of c-Si/Al_2O_3, under the assumption that similar D_{it} and Q_{ss} can be expected. Figure 6 shows the values of D_{it} and Q_{ss} determined as a function of annealing time. In the absence of thermal annealing, the Q_{ss} at 400 and 500 °C was found to be 5.27×10^{10} and 1.0×10^{10} cm^{-3}, respectively. We used different samples for the annealing experiments at 400 and 500 °C, and therefore, a small difference in the observed values of Q_{ss} was expected. The relationship between the surface recombination velocity and Q_{ss} was established as follows: the results showed that low values of Q_{ss} (below 10^{11} cm^{-3}) did not reduce the surface recombination velocity [25]. As shown in Fig. 7a, Q_{ss} increased drastically after annealing. The Al_2O_3 layer fabricated on the Si generates negatively charged Al vacancies in the vicinity of the interface [23, 26]. The formation of Al vacancies represents one of the possible explanations for the origin of the negative fixed charge at the Al_2O_3/c-Si interface. The samples annealed at 400 and 500 °C exhibited almost identical Q_{ss}. Therefore, the decrease in τ_{eff} cannot be explained by the values of Q_{ss}. Figure 6b illustrates that D_{it} varied significantly with changes in the annealing temperature. For example, while the D_{it} at 400 °C was found to decrease with increasing time, the D_{it} at 500 °C exhibited the opposite trend. At the annealing time at 400 °C, the hydrogen from Al_2O_3 and FG can connect to the dangling bond. At annealing temperatures above 500 °C, on the other hand, the dangling bonds on the Si surface are generated as a result of bond disconnection between Si and H [27]. The results of our analysis showed that the value of τ_{eff} as a function of time was affected by the time-variable parameter D_{it}. These results indicate that the SiNWs/Al_2O_3 annealing conditions significantly affect the interface quality.

Conclusions

We investigated the influence of SiNW fabrication and annealing procedures on the effective lifetime of SiNW/Al_2O_3 samples. Complete crystallization of SiNWs is essential to obtain a high effective lifetime, in particular, because the a-Si phase remaining in the material can

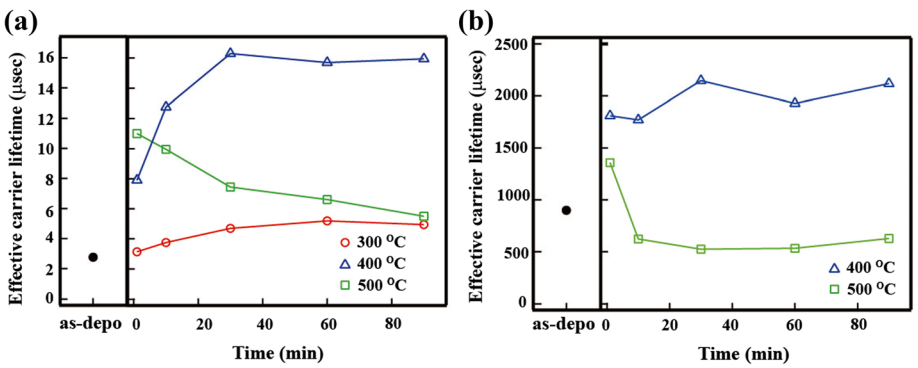

Fig. 6 **a** Dependence of τ_{eff} of SiNWs/Al_2O_3 on annealing time and temperature. **b** Dependence of τ_{eff} of c-Si/Al_2O_3 on annealing time and temperature

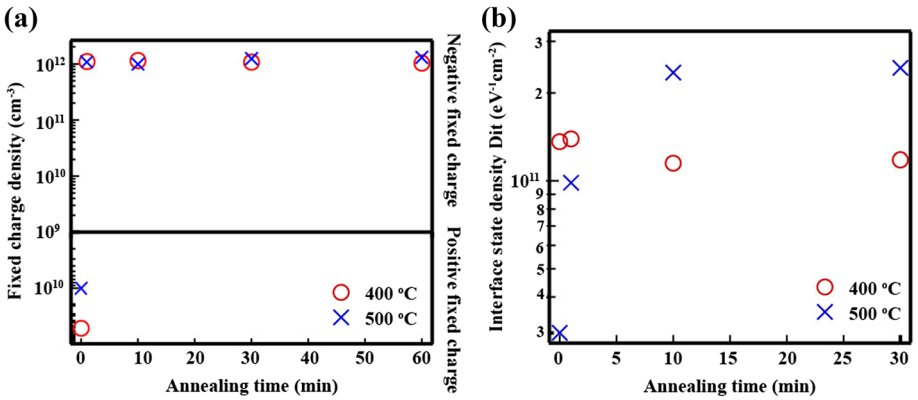

Fig. 7 **a** Fixed-charge density (Q_{ss}) and **b** interface-state density (D_{it}) as a function of annealing time for different annealing temperature (400 and 500 °C)

result in a decrease in the bulk lifetime of SiNWs. Here, fully crystallized thin-layer SiNWs were obtained by MAE of large-grain poly-Si. Through thermal annealing at 400 °C for 30 min in a forming gas, the effective lifetime of SiNWs/Al_2O_3 drastically improved from 2.86 to 15.9 μs. By comparing the effective lifetime of SiNWs/Al_2O_3 and c-Si/Al_2O_3 samples, we concluded that the thermal annealing conditions, especially temperature, significantly affect the state density at the SiNW/Al_2O_3 interface.

Abbreviations

Al_2O_3: Aluminum oxide; MAE: Metal-assisted chemical etching; MWPCD: Microwave photoconductivity decay; SiNWs: Silicon nanowires; SPC: Solid phase crystallization; τ_{eff}: Effective carrier lifetime

Acknowledgements

This work was supported in part by the Ministry of Education, Culture, Sports, Science and Technology (MEXT) and FUTURE-PV Innovation.

Authors' Contributions

SK carried out the experiment and wrote the initial draft of the manuscript. TY contributed to the sample fabrication and sample measurement. SM supervised the work and finalized the manuscript. YK and MK gave the final approval of the version of the manuscript to be published. All authors read and approved the final manuscript.

Competing Interests

The authors declare that they have no competing interests.

Publisher's Note

Author details

[1]Department of Electrical and Mechanical Engineering, Nagoya Institute of Technology, Showa-ku, Nagoya-shi, Aichi 466-8555, Japan. [2]Department of Physical Electronics, Tokyo Institute of Technology, Meguro-ku, Tokyo 152-8552, Japan. [3]Graduate School of Engineering, Nagoya University, Nagoya, Aichi 464-8603, Japan. [4]Department of Electrical and Electronic Engineering, Tokyo Institute of Technology, Meguro-ku, Tokyo 152-8552, Japan. [5]Advanced Research laboratories, Tokyo City University, Setagaya-ku, Tokyo 158-0082, Japan. [6]FUTURE-PV Innovation, Japan Science and Technology Agency (JST), Koriyama, Fukushima 963-0215, Japan.

Received: 5 December 2016 Accepted: 17 March 2017
Published online: 31 March 2017

References

1. Kato S, Kurokawa Y, Watanabe Y, Yamada Y, Yamada A, Ohta Y et al (2013) Optical assessment of silicon nanowire arrays fabricated by metal-assisted chemical etching. Nanoscale Res Lett 8: 216
2. Lin CX, Povinelli ML (2009) Optical absorption enhancement in silicon nanowire arrays with a large lattice constant for photovoltaic applications. Opt Express 17:19371–19381
3. Kurokawa Y, Kato S, Watanabe Y, Yamada A, Konagai M, Ohta Y et al (2012) Numerical approach to the investigation of performance of silicon nanowire solar cells embedded in a SiO2 matrix. Jpn J Appl Phys 51:11PE12-1 -11PE12-4
4. Wang X, Peng KQ, Pan XJ, Chen X, Yang Y, Li L et al (2011) High-performance silicon nanowire array photoelectrochemical solar cells through surface passivation and modification. Angew Chem Int Ed 50:9861–9865
5. Yu P, Wu J, Liu ST, Xiong J, Jagadish C, Wang ZMM (2016) Design and fabrication of silicon nanowires towards efficient solar cells. Nano Today 11:704–737
6. Zhang ML, Peng KQ, Fan X, Jie JS, Zhang RQ, Lee ST et al (2008) Preparation of large-area uniform silicon nanowires arrays through metal-assisted chemical etching. J Phys Chem C 112:4444–4450
7. Ishikawa R, Kato S, Yamazaki T, Kurokawa Y, Miyajima S, Konagai M (2014) Solid-phase crystallization of amorphous silicon nanowire array and optical properties. Jpn J Appl Phys 53:02BE09-1 - 02BE09-4
8. Yamazaki T, Kato S, Miyajima S, Konagai M (2014) Minority carrier lifetime of thin polycrystalline silicon nanowire films on polycrystalline silicon layer prepared by aluminum-induced crystallization. Next Generation Technologies for Solar Energy Conversion V 9178:91780L-1 - 9178L-7
9. Kato S, Yamazaki T, Miyajima S, Konagai M (2014) Influence of substrates on formation of polycrystalline silicon nanowire films. Next Generation Technologies for Solar Energy Conversion V 9178:91780M-1 - 91780M-6
10. Brodoceanu D, Alhmoud HZ, Elnathan R, Delalat B, Voelcker NH, Kraus T (2016) Fabrication of silicon nanowire arrays by near-field laser ablation and metal-assisted chemical etching. Nanotechnology 27:075301-1 - 075301-8
11. Zhang SL, Wang XW, Liu H, Shen WZ (2014) Controllable light-induced conic structures in silicon nanowire arrays by metal-assisted chemical etching. Nanotechnology 25:025602-1 - 025602-11
12. Brody J, Rohatgi A, Ristow A (2003) Review and comparison of equations relating bulk lifetime and surface recombination velocity to effective lifetime measured under flash lamp illumination. Sol Energy Mater Sol Cells 77:293–301
13. Lauer K, Laades A, Ubensee H, Metzner H, Lawerenz A (2008) Detailed analysis of the microwave-detected photoconductance decay in crystalline silicon. J Appl Phys 104:104503-1 - 104503-9
14. Ogita YI (1996) Bulk lifetime and surface recombination velocity measurement method in semiconductor wafers. J Appl Phys 79:6954–6960

15. Kato S, Kurokawa Y, Miyajima S, Watanabe Y, Yamada A, Ohta Y et al (2013) Improvement of carrier diffusion length in silicon nanowire arrays using atomic layer deposition. Nanoscale Res Lett 8:361
16. Sivakov V, Andra G, Gawlik A, Berger A, Plentz J, Falk F et al (2009) Silicon nanowire-based solar cells on glass: synthesis, optical properties, and cell parameters. Nano Lett 9:1549–1554
17. Kato S, Watanabe Y, Kurokawa Y, Yamada A, Ohta Y, Niwa Y et al (2012) Metal-assisted chemical etching using silica nanoparticle for the fabrication of a silicon nanowire array. Jpn J Appl Phys 51:02BP09-1 - 02BP09-4
18. Hirasawa M, Orii T, Seto T (2006) Size-dependent crystallization of Si nanoparticles. Appl Phys Lett 88:093119-1 - 093119-3
19. Mishra P, Jain KP (2000) Temperature-dependent Raman scattering studies in nanocrystalline silicon and finite-size effects. Physical Review B 62:14790–14795
20. Kanzawa Y, Kageyama T, Takeoka S, Fujii M, Hayashi S, Yamamoto K (1997) Size-dependent near-infrared photoluminescence spectra of Si nanocrystals embedded in SiO_2 matrices. Solid State Commun 102:533–537
21. Agostinelli G, Delabie A, Vitanov P, Alexieva Z, Dekkers HFW, De Wolf S, et al (2006) Very low surface recombination velocities on p-type silicon wafers passivated with a dielectric with fixed negative charge. Solar Energy Mater and Solar Cells 90:3438–3443
22. Hoex B, Schmidt J, Pohl P, van de Sanden MCM, and Kessels WMM (2008) Silicon surface passivation by atomic layer deposited Al(2)O(3). J Appl Phys 104:044903-1 - 044903-12
23. Hoex B, Gielis JJH, de Sanden MCMV, Kessels WMM (2008) On the c-Si surface passivation mechanism by the negative-charge-dielectric Al2O3. J Appl Phys 104: 113703-1 - 113703-7
24. Dingemans G, Seguin R, Engelhart P, van de Sanden MCM, Kessels WMM (2010) Silicon surface passivation by ultrathin Al2O3 films synthesized by thermal and plasma atomic layer deposition. Physica Status Solidi-Rapid Res Lett 4: 10–12
25. Miyajima S (2009) Surface passivation films for crystalline silicon solar cells. The Japan Society of Plasma Science and Nuclear Fusion Research 85:820–824
26. Naumann V, Otto M, Wehrspohn RB, Werner M, Hagendorf C (2012) Interface and material characterization of thin ALD-Al2O3 layers on crystalline silicon. Proc 2nd Int Conf Crystalline Silicon Photovoltaics 27: 312–318
27. Cantin JL, von Bardeleben HJ (2002) An electron paramagnetic resonance study of the Si(100)/Al2O3 interface defects. J Non Cryst Solids 303:175–178